

# NRF2 regulates endothelial glycolysis and proliferation with miR-93 and mediates the effects of oxidized phospholipids on endothelial activation

Suvi M. Kuosmanen<sup>1</sup>, Emilia Kansanen<sup>1</sup>, Minna U. Kaikkonen<sup>1</sup>, Virve Sihvola<sup>1</sup>, Kati Pulkkinen<sup>1</sup>, Henna-Kaisa Jyrkkänen<sup>1</sup>, Pauli Tuoresmäki<sup>2</sup>, Juha Hartikainen<sup>3,4</sup>, Mikko Hippeläinen<sup>4</sup>, Hannu Kokki<sup>3,5</sup>, Pasi Tavi<sup>1</sup>, Sami Heikkinen<sup>2</sup> and Anna-Liisa Levenon<sup>1,\*</sup>

<sup>1</sup>A.I. Virtanen Institute for Molecular Sciences, University of Eastern Finland, 70211 Kuopio, Finland, <sup>2</sup>Institute of Biomedicine, School of Medicine, University of Eastern Finland, 70211 Kuopio, Finland, <sup>3</sup>School of Medicine, University of Eastern Finland, 70211 Kuopio, Finland, <sup>4</sup>Heart Centre, Kuopio University Hospital, 70211 Kuopio, Finland and <sup>5</sup>Anaesthesia and Operative Services, 70211 Kuopio University Hospital, Kuopio, Finland

Received September 07, 2017; Revised October 12, 2017; Editorial Decision October 29, 2017; Accepted November 01, 2017

## ABSTRACT

Phospholipids, such as 1-palmitoyl-2-arachidonoyl-*sn*-glycero-3-phosphocholine (PAPC), are the major components of cell membranes. Their exposure to reactive oxygen species creates oxidized phospholipids, which predispose to the development of chronic inflammatory diseases and metabolic disorders through endothelial activation and dysfunction. Although the effects of oxidized PAPC (oxPAPC) on endothelial cells have been previously studied, the underlying molecular mechanisms evoking biological responses remain largely unknown. Here, we investigated the molecular mechanisms of oxPAPC function with a special emphasis on NRF2-regulated microRNAs (miRNAs) in human umbilical vein endothelial cells (HUVECs) utilizing miRNA profiling, global run-on sequencing (GRO-seq), genome-wide NRF2 binding model, and RNA sequencing (RNA-seq) with miRNA overexpression and silencing. We report that the central regulators of endothelial activity, KLF2 for quiescence, PFKFB3 for glycolysis, and VEGFA, FOXO1 and MYC for growth and proliferation, are regulated by transcription factor NRF2 and the NRF2-regulated miR-106b~25 cluster member, miR-93, in HUVECs. Mechanistically, oxPAPC was found to induce glycolysis and proliferation NRF2-dependently, and oxPAPC-dependent induction of the miR-106b~25 cluster was mediated by NRF2. Additionally, several regulatory loops were established between NRF2, miR-93 and the essential regulators of healthy endothelium, collectively implying that

**NRF2 controls the switch between the quiescent and the proliferative endothelial states together with miR-93.**

## INTRODUCTION

The inner lining of the vascular wall consists of a single layer of endothelial cells. The layer acts as a barrier between the circulating blood and the underlying tissues, as well as a key regulator of cardiovascular homeostasis and protector against vascular diseases (1). Risk factors for vascular diseases, such as hyperlipidemia, hypertension and diabetes, increase both endothelial and vascular reactive oxygen species (ROS) production, which can cause lipid peroxidation and promote endothelial dysfunction (1,2). In normal cell physiology, ROS produced in response to various exogenous and endogenous stimuli is constantly transformed and consumed by tissue metabolism, and a careful balance between ROS-generating pro-oxidants and their elimination with antioxidants maintains the redox homeostasis. The cellular defence against ROS is based on antioxidants, many of which are regulated by the transcription factor nuclear factor E2-related factor 2 (NRF2), which is induced by oxidative stress (3).

1-Palmitoyl-2-arachidonoyl-*sn*-glycero-3-phosphocholine (PAPC) is abundant phospholipid in cell membranes and lipoproteins. Due to its surface location, it is prone to oxidation generating an array of oxidation products, collectively referred to as oxPAPC. OxPAPC is a strong mediator of endothelial activation stimulating sprouting and tubulogenesis in cell models and angiogenesis in animal models (4–6). OxPAPC has been reported to protect barrier function and to activate Nuclear factor erythroid 2-Related Factor 2 (NRF2) pathway, thus increasing the endothelial tolerance to oxidative stress

\*To whom correspondence should be addressed. Tel: +358 40 358 9907; Email: anna-liisa.levenon@uef.fi

and inflammation (7,8). The exact mechanism for NRF2 pathway activation by oxPAPC is not known, but is likely to be mediated by the covalent modification of reactive cysteine residues of Kelch ECH-associating protein 1 (KEAP1) by electrophilic lipid mediators within oxPAPC (7,9). Two KEAP1 molecules form the core of the NRF2 inhibitory complex, which in basal state mediates the proteasomal degradation of NRF2 (10). Inactivation of the inhibitory complex by oxPAPC would lead to accumulation of *de novo* synthesized NRF2 and induction of its target gene expression. In addition to cytoprotective and anti-inflammatory genes, oxPAPC can also upregulate genes involved in inflammation and pro-coagulant activity (4). Although the modulatory effect of oxidized phospholipids in biological processes is recognized, the underlying molecular mechanisms remain elusive.

MicroRNAs (miRNAs) regulate various aspects of endothelial function, and have been shown to mediate oxidized phospholipid signalling in endothelial cells (11–15). miRNAs elicit their function at the post-transcriptional level fine-tuning the expression of protein-encoding genes by suppressing protein synthesis or initiating mRNA degradation. Furthermore, miRNAs can become selectively enriched in secretory nanovesicles, exosomes, and mediate communication with remote cells thus affecting the function of multiple cell types (11,16,17). However, many aspects of miRNA biology are still unknown and their transcriptional regulation is poorly described. Interestingly, a recent study that mapped transcription start sites for human miRNAs in DROSHA knockout cells revealed a significant enrichment of small MAF and BACH1 binding sites, which also bind NRF2, on putative miRNA promoters suggesting NRF2 to be a common regulator of miRNA function (18).

In this study, we set out to identify novel oxPAPC-responsive NRF2-regulated miRNAs with endothelial relevance in order to enlighten the mechanisms through which oxidized phospholipids evoke the quiescent endothelium. To this end, we utilized global miRNA profiling (miRNA array and miRNA sequencing), global run-on sequencing (GRO-seq), previously published genome-wide NRF2 binding model (15), and RNA sequencing (RNA-seq) with miRNA overexpression and silencing. We report that the central regulators of endothelial function, Krüppel-like factor 2 (KLF2) for quiescence, 6-phosphofructo-2-kinase/fructose-2,6-biphosphatase 3 (PFKFB3) for glycolysis, and Vascular Endothelial Growth Factor A (VEGFA), Forkhead box protein O1 (FOXO1) and MYC proto-oncogene protein (MYC) for growth and proliferation, respond to oxPAPC treatment and are regulated by the transcription factor NRF2 and the NRF2-regulated miR-106b~25 cluster member, miR-93, in human umbilical vein endothelial cells (HUVECs). Furthermore, we show that oxPAPC induces glycolysis and proliferation, as well as miR-106b~25 cluster expression, NRF2-dependently. Taken together, we have shown for the first time the impact of miR-93 and NRF2 on endothelial glycolysis and their interplay with other mediators of endothelial quiescence, glycolysis, and angiogenesis.

## MATERIALS AND METHODS

### Cell culture

Umbilical cords were obtained from the maternity ward of the Kuopio University Hospital, and the Human Umbilical Vein Endothelial Cells (HUVECs) were extracted with collagenase (0.3mg/ml) digestion. Research Ethics Committee of the Hospital District of Northern Savo, Kuopio, Finland approved the collection. The cells were cultivated in Endothelial Cell Basal Medium (Lonza) with recommended supplements (EGM SingleQuot Kit Supplements & Growth Factors, Lonza). Cells of 18 different donors were used in the study. The essential results were repeated on at least three donor batches (on passages 4–6).

### Patient samples and sample preparation

Pericardial fluid samples (2–27ml) were collected during open-heart surgery and processed immediately after sample collection. A written informed consent was obtained from each participant. Research Ethics Committee of the Hospital District of Northern Savo, Kuopio, Finland approved the study. Briefly, pericardial fluid samples were collected from 48 subjects (Supplementary Table S1) with coronary artery disease, mitral valve insufficiency, aortic stenosis, or aortic valve insufficiency. Patients were also grouped according to the NYHA class (New York Heart Association functional classification) for the extent of heart failure (HF): patients without clinical HF belong to group 0 ( $n=3$ ), patients with cardiac disease but no symptoms and no limitations in ordinary physical activity in group I ( $n=4$ ), patients with mild symptoms in group II ( $n=18$ ), patients with marked limitation in activity due to symptoms in group III ( $n=12$ ), and patients with severe limitations and symptoms even while resting in group IV ( $n=11$ ). Samples were processed directly after sample collection using three-step centrifugation. Samples were first centrifuged at 300g for 10min at RT to remove cells. Then, the supernatants were collected and centrifuged again at 16,500g for 20min at 4°C to remove cell debris. The collected liquid fractions were centrifuged a final time at 20,000g for 15min at 4°C to remove other microparticles, leaving exosomes and protein-bound miRNAs to the supernatants. The supernatants were transferred to RNase-free tubes, snap-frozen with liquid nitrogen and stored at –80°C.

### Reagents

1-palmitoyl-2-archidonoyl-*sn*-glycero-3-phosphocholine (PAPC, 10mg/ml) was purchased from Avanti Polar Lipids, Inc, oxidized to oxPAPC by exposure to air for 40h, dissolved in chloroform and stored at –70°C. Upon use, the chloroform was evaporated with nitrogen (g) and the lipids were re-suspended in growth medium. For experiments, concentration of 30µg/ml was used, except for glycolysis experiments, where 20µg/ml was used.

### RNA extraction and qRT-PCR

Total fluid RNA was extracted using miRCURY RNA Isolation Kit for Biofluids (Exiqon). Exosomes were isolated

using miRCURY Exosome Isolation Kit (Exiqon), and total RNA (both cellular and exosomal) was isolated using miRCURY RNA isolation kit for cells and plants (Exiqon). Non-exosomal RNA was isolated from the medium after exosome isolation using miRCURY RNA Isolation Kit for Biofluids (Exiqon).

miRNAs were reverse transcribed using miRCURY LNA Universal RT miRNA PCR, polyadenylation and cDNA synthesis kit (Exiqon) and mRNA with Transcriptor First Strand cDNA Synthesis Kit (Roche). cDNA templates were assayed in 10  $\mu$ l PCR reactions with either LightCycler 96 System or LightCycler 480 Real-Time PCR System (Roche) according to the protocol of miRCURY LNA Universal RT miRNA PCR for miRNA samples and the protocol of Fast Start Universal Probe Master (Rox) (Roche) for mRNA samples. miRNA levels were determined using hsa-miR-106b-5p (205884, Exiqon), -3p (204020, Exiqon), hsa-miR-93-5p (204715, Exiqon), -3p (204470, Exiqon), hsa-miR-25-5p (204031, Exiqon), -3p (204361, Exiqon) LNA<sup>TM</sup> PCR primer sets. mRNA levels were determined using Universal Probe Library System (Roche, specific primer-probe pairs are listed in Supplemental Material) and Assays-on-Demand target mixtures for *MCM7* (Hs00428518, Applied Biosystems) and *PPIA* (Hs04194521\_s1, Applied Biosystems). For analysis, Roche LC Software was used for Cp determination (by the second derivative method) and for melting curve analysis (miRNA samples). *GAPDH* and *PPIA* were used for normalisation.

### MicroRNA array

The samples were treated with oxPAPC (30  $\mu$ g/ml) for 4h in EGM or with fresh EGM (control). Total RNA was extracted with TriReagent (Sigma-Aldrich). The profiling and data analysis was executed at Exiqon Services, Denmark. The quality of the total RNA was verified by an Agilent 2100 Bioanalyzer profile. 200ng total RNA from sample and reference was labelled with Hy3<sup>TM</sup> and Hy5<sup>TM</sup> fluorescent label, respectively, using the miRCURY<sup>TM</sup> LNA Array power labelling kit (Exiqon, Denmark) following the procedure described by the manufacturer. The Hy3<sup>TM</sup>-labeled samples and a Hy5<sup>TM</sup>-labeled reference RNA sample were mixed pair-wise and hybridized to the miRCURY<sup>TM</sup> LNA array version 11.0 (Exiqon, Denmark), which contained capture probes targeting all miRNAs for human, mouse or rat registered in the miRBASE version 13.0 at the Sanger Institute. The hybridisation was performed according to the miRCURY<sup>TM</sup> LNA array manual using a Tecan HS4800 hybridisation station (Tecan, Austria). After hybridisation the microarray slides were scanned and stored in an ozone free environment (ozone level below 2.0ppb) in order to prevent potential bleaching of the fluorescent dyes. The miRCURY<sup>TM</sup> LNA array microarray slides were scanned using the Agilent G2565BA Microarray Scanner System (Agilent Technologies, Inc., USA) and the image analysis was carried out using the ImaGene 8.0 software (BioDiscovery, Inc., USA). The quantified signals were background corrected (Normexp with offset value 10 (19)) and normalized using the global Lowess (LOcally WEighted Scatterplot Smoothing) regression algorithm.

### Global run-on sequencing

HUVECs were grown to 80% confluency on 15cm plates and treated with oxPAPC (30  $\mu$ g/ml) for 6 hours in 1% FBS EGM or with fresh 1% FBS EGM (control). To collect nuclei for GRO-Seq, cells were washed once with PBS, trypsinized for 30s, neutralized with ice-cold swelling buffer (10mM Tris-HCl, 2mM MgCl<sub>2</sub>, 3mM CaCl<sub>2</sub> and 2U/ml SUPERase Inhibitor, Thermo Fisher Scientific) and collected by scraping. Nuclei were prepared as described in (20) and ~5 million nuclei were recovered and subjected to run-on reaction. GRO-seq libraries were prepared as previously described with minor modifications (21). Briefly, the run-on products were base hydrolyzed (RNA fragmentation reagent, Thermo Fisher Scientific), end-repaired using polynucleotide kinase and immunoprecipitated with anti-BrdU agarose beads (Santa Cruz, CA, USA) in binding buffer (0.5  $\times$  SSPE, 1 mM EDTA, 0.05% Tween-20) for 1h at RT. Beads were washed twice with ice cold binding buffer and low salt buffer (0.2  $\times$  SSPE, 1 mM EDTA, 0.05% Tween-20), once with high salt buffer (0.5% SSPE, 1 mM EDTA, 0.05% Tween-20, 150mM NaCl) and twice with TET buffer (TE pH 7.4, 0.05% Tween-20). The captured RNA was eluted with 3  $\times$  100  $\mu$ l elution buffer (20 mM DTT, 300 mM NaCl, 5mM Tris pH 7.5, 1 mM EDTA and 0.1% SDS), purified using Trizol-LS protocol (Thermo Fisher Scientific), ethanol precipitated and subjected to second round of immunoprecipitation. The immunopurified RNA was eluted as above and ethanol precipitated. The following day, a poly-A tailing reaction (PolyA polymerase, New England Biolabs, Ipswich, MA, USA), cDNA synthesis (Superscript III, Thermo Fisher Scientific), Exonuclease I (New England Biolabs) treatment, purification using ChIP DNA Clean & Concentrator Kit (Zymo Research Corporation, Irvine, CA, USA), RNaseH treatment and circularisation (CircLigase, Illumina), were performed. The libraries were amplified for 13 cycles and library band was excised (~200–350 bp) from 10% NOVEX TBE gel (Thermo Fisher Scientific). The libraries were quantified (Qubit ds-DNA HS Assay Kit on a Qubit fluorometer, Thermo Fisher Scientific) and pooled for 50bp single-end sequencing with Illumina Hi-Seq2000 (GenCore, EMBL Heidelberg, Germany).

### MicroRNA sequencing

HUVECs were isolated from umbilical cords as described in (22). Total RNA was extracted using miRCURY RNA isolation kit for cells and plants (Exiqon). miRNA profiling was executed at Exiqon Services, Denmark. 300ng RNA was used for miRNA library preparation using NEBNext library generation kit (New England Biolabs) according to the manufacturer's protocol. Libraries were purified on QiaQuick columns and the insert efficiency was evaluated by Bioanalyzer 2100 instrument on high sensitivity DNA chip (Agilent Inc.). miRNA cDNA libraries were size fractionated on a LabChip XT (Caliper) and a band of correct size was excised using the manufacturer's instructions. Libraries were pooled in equimolar concentrations and optimal concentration of the library pool was used to generate the clusters on the surface of a flowcell before sequencing using v3

sequencing methodology according to the manufacturer instructions (Illumina). miRNA-seq libraries were sequenced on Illumina NextSeq 500 system according to the manufacturer's instructions. The data was mapped to miRBase (v20) (23) and to genome version GRCh37 using Bowtie2 (2.2.2) (24). The aligned reads were required to match the reference sequence perfectly and one mismatch was allowed in the first 32 bases of the read when mapping to the genome. No indels were allowed in the mapping. The differential expression analysis was performed using the EdgeR statistical software package (25,26).

### Transductions

The pAd-KEAP1 was cloned by excising the BamHI-XhoI fragment containing the human KEAP1 cDNA from pCDNA3 and ligating the fragment into pAdCMV. The constructs were then used to generate the recombinant adenoviruses using standard techniques (27). For transduction, HUVECs were seeded onto 6-well plates at the density of 180,000 cells/well and allowed to adhere for 24h. The cells were transduced in serum-free conditions with AdCMV (28), AdNRF2 (28) or AdKEAP1. The multiplicity of infection (MOI) was 100 in all experiments. After an hour, cell culture supplements were added, and after additional 16h the transduced cells were washed with PBS and fresh medium with full supplements was added. Gene expression, Western blot, metabolism and proliferation analyses were performed 48h after transductions.

### Chromatin immunoprecipitation (ChIP)

ChIP was performed as previously described in (15). ChIP templates were assayed in 10 $\mu$ l qPCR reactions with a LightCycler 96 System (Roche) according to the FastStart Universal SYBR Green Master (Rox) (Roche) protocol using chromatin region-specific primers listed in Supplemental Material. For analysis, Roche LC Software was used for Cp determination (by the second derivative method) and for melting curve analysis. The results were calculated relative to control treatment values.

### Transfections

MISSION miRNA Mimics Negative Control #1 (HMC0002, Sigma-Aldrich), hsa-miR-93-5p mimic (HMI0960, Sigma-Aldrich), MISSION Synthetic microRNA (miRNA) Inhibitors Negative control I (NCSTUD001, Sigma-Aldrich), hsa-miR-93-5p inhibitor (HSTUD0960, Sigma-Aldrich), High GC duplex negative control (46-2000, Invitrogen), KLF2 (siRNA ID 116130, AM16708, Ambion) and NRF2 (5'-UGACAGAAGUUGACAAUUA-3') siRNAs were transfected into cells using Oligofectamine (Invitrogen) in EBM. After 4h, supplements were added, and the next day the transduced cells were washed with PBS and fresh medium with full supplements was added. Mimic, inhibitor and siRNA concentrations used in all experiments were 25, 1 and 12nM, respectively. Gene expression, RNA-seq, western blot, metabolism and proliferation analyses were performed 48h after transfection.

### RNA sequencing

RNA-seq libraries were prepared as described in (21,29). Briefly, RNA was purified using Trizol and enriched for Poly(A)-RNA with MicroPoly(A) Purist Kit (Life Technologies). RNA was treated with TURBO DNase (Life Technologies), fragmented using RNA Fragmentation Reagents (Life Technologies) and purified with P-30 column (Bio-Rad). The 3' end of the fragmented RNA was dephosphorylated with T4 polynucleotide kinase (PNK; New England Biolabs) followed by heat-inactivation. Dephosphorylation reactions were purified with gel extraction on Novex 10% polyacrylamide TBE-urea gel (Life Technologies). Poly(A)-tailing and cDNA synthesis were performed the next day. RNA fragments were subjected to poly-A tailing reaction in 8.0 $\mu$ l volume containing 0.8 $\mu$ l poly-A polymerase buffer, 1 $\mu$ l 1 mM ATP, 0.5 $\mu$ l of SUPERase-In, and 0.75 $\mu$ l poly-A polymerase (New England Biolabs). The reaction was carried out for 30min at 37°C. Tailed RNA (8.0 $\mu$ l) was mixed with 1 $\mu$ l dNTP (10mM each) and 2.5 $\mu$ l 12.5 $\mu$ M primer (5Phos/GATCGTCCGACTGTAGA ACTCTGAAC/IS p18/TCAGACGTGTGCTCTTCCGATCTTTTTTTTTTT TTTTTTTTTTVN (IDT)), heated for 3min at 75°C, and chilled briefly on ice. Then, 0.5 $\mu$ l SUPERase-In, 3 $\mu$ l 0.1M DTT, 2 $\mu$ l 25mM MgCl<sub>2</sub>, 2 $\mu$ l 10 $\times$  reverse transcription buffer and 1 $\mu$ l superscript III reverse transcriptase were added (Invitrogen). The tube was incubated for 30min at 48°C. After cDNA synthesis, Exonuclease I (New England Biolabs) was used to catalyze the removal of excess oligo. The DNA-RNA hybrid was purified using ChIP DNA Clean & Concentrator Kit (Zymo Research Corporation, Irvine, CA, USA), RNaseH treated and circularized. The libraries were amplified for 11–14 cycles with oNTI201-primer: 5'-AATGATACGGCGACCACCGACAGGT TCAGAGTTCTACAGTCCGACG-3' and a barcode specific primer oNTI200-index: 5'-CAAGCAGAAGACG GCATACGAGATXXXXXXGTGACTGGAGTTCAGACGTGTGCTCTTCCGATCT (barcode XXXXXX). The final product was ran on Novex 10% TBE gel, purified and cleaned up as above. The libraries were sequenced on the Illumina HiSeq 2000 according to the manufacturer's instructions. RNA-seq data was mapped using TopHat2 (30) with underlying Bowtie2 (24) allowing one mismatch and one alignment for each read, and visualized by preparing custom tracks for the Integrative Genomics Viewer (IGV) with igvtools (31,32). Differentially expressed genes were identified using DESeq2 (33), and required to have adjusted *P*-values <0.05. Ingenuity Pathway Analysis (IPA, Qiagen Redwood City, [www.qiagen.com/ingenuity](http://www.qiagen.com/ingenuity)) was used to identify affected canonical pathways and biological functions. Both significantly up- and down-regulated genes were entered to the analysis.

### Proliferation assay

HUVECs were seeded on 96-well plates (Corning Costar Assay Plate, Black) 8,000 cells per well, and cell proliferation was measured in various conditions using CyQUANT Direct Cell Proliferation Assay Kit (Invitrogen) following the assay protocol. OxPAPC treatment (30 $\mu$ g/ml) time was 48h.

## Glycolytic activity

Glycolytic activity was measured using Seahorse XF24 analyzer (Seahorse Bioscience). HUVECs were seeded overnight (60,000) cells per well on fibronectin-gelatin-coated Seahorse XF24 microplates, and maintained in non-buffered assay medium in non-CO<sub>2</sub> incubator for 30min before the assay. The extracellular acidification rate (ECAR) was measured over 4min periods with a mixing of 2min in each cycle with five cycles in total. Activators and inhibitors (from Sigma) were injected after each cycle and were used at the following concentrations: Glucose (10mM), Oligomycin (1μM), 2-DG (100mM). Cellular protein concentration was measured using Bio-Rad Protein Assay (Bio-Rad). The data is represented as ECAR normalized to protein concentration. OxPAPC treatment time was 24h prior glycolysis measurements. Glycolytic rate is the ECAR rate reached by the cell population after the addition of saturating amounts of glucose. Glycolytic capacity is the maximum ECAR rate reached by the cell population after oligomycin addition, which shuts down oxidative phosphorylation and drives the cell to use glycolysis to its maximum capacity.

## RNA pull-down with biotinylated miRNA mimics

HUVECs were grown to 70% confluency on 10cm plates. RNA pull down was performed as described in (<https://doi.org/10.1101/005439>) using biotinylated hsa-miR-93-5p (miRCURY LNA microRNA mimics, Premium, Biotin, Exiqon) and biotinylated control miRNA (cel-miR-39-3p, miRCURY LNA microRNA mimics, Premium, Biotin, Exiqon). Transfections were performed, as described above with oligofectamin, and the pull-down experiments were performed 48h after transfection. OxPAPC treatment (30μg/ml) time for all experiments was 8h. RNA was extracted from the beads using miRCURY RNA isolation kit for cells and plants (Exiqon). RNA was reverse transcribed and cDNA templates were assayed in 10μl PCR reactions. The primers used for sample quantitation are listed in a table in **Supplemental Material**.

## Western blot

HUVECs were grown on six-well plates. Cells were lysed in WB lysis buffer (50mM Tris-HCl, 150mM NaCl, 1 mM EDTA, 1% Triton X-100, 0.5% Na-deoxycholate, 0.1% SDS, 10% Glycerol, pH 7.5) containing protease inhibitors (Roche), resolved by SDS-PAGE, transferred to nitrocellulose membrane, and probed with indicated antibodies: KLF2 (sc-18690, Santa Cruz Biotechnologies), NRF2 (sc-13032, Santa Cruz Biotechnologies), PFKFB3 (#13123, Cell Signaling Technology), FOXO1 (#2880, Cell Signaling Technology), c-MYC (#9402, Cell Signaling Technology), β-actin (#4967L, Cell Signaling Technology and sc-47778, Santa Cruz Biotechnologies), ECL Plex goat-α-rabbit IgG, CY5 (Pa45012V, GE Healthcare) and ECL Plex goat-α-mouse IgG, CY3 (PA43010V, GE Healthcare). Rat monoclonal Keap1 antibody (clone 144) was a generous gift from Dr. Ken Itoh (Centre for Advanced Medical Research, Hiroshima University Graduate School of Medicine, Japan)

## Statistical analyses

All experiments were performed at least three times with at least three biological replicates per experiment, exception being RNA-seq, which was obtained from 2–3 biological replicates per sample group. Statistical significance was evaluated with unpaired, two-tailed Student's test (\* $P < 0.05$ , \*\* $P < 0.01$ , \*\*\* $P < 0.001$ , \*\*\*\* $P < 0.0001$ ). Results are expressed as mean ± SD, except for glycolysis rate diagrams, for which mean ± SEM was used for visual clarity.

## RESULTS

### miRNA selection

NRF2 is a known mediator of oxPAPC response (7). OxPAPC treatment in endothelial cells leads to accumulation of both cellular and nuclear NRF2, which is a sign of NRF2 response (Supplementary Figures S1A-B). In order to identify novel oxPAPC-responsive NRF2-regulated miRNAs with endothelial relevance, two oxPAPC datasets, miRNA array and GRO-seq, were utilized together with previously published NRF2 binding model (15) (Figure 1). The miRNA array indicated 19 significantly ( $P < 0.01$ ) altered mature miRNAs arising from 18 genomic loci (Figure 1A, Supplementary Table S2). Nine of these loci were confirmed to be oxPAPC-responsive also on transcriptional level based on GRO-seq data, and five of the loci were predicted to be NRF2-regulated by previously published NRF2 binding model (15) (Figure 1A). The criteria for the binding model selection was that at least one 'medium-to-strong' binding site (as determined in (15)) had to reside on active enhancer/promoter element in HUVECs within ±5,000 bp from the miRNA or miRNA cluster locus. In addition to two previously characterized NRF2-regulated miRNA loci, namely *MIR126* and *MIR125b* (15,34), the five candidate loci contained two miRNA clusters, a well-characterized miR-23-27-24 cluster and a more unknown miR-106b~25 cluster, which was chosen for further studies (Figure 1B and C).

### NRF2 regulates miR-106b~25 cluster expression and response to oxidized phospholipids

miR-106b~25 cluster is located at the 13th intron of the *minichromosome maintenance complex component 7* (*MCM7*) gene on chromosome 7 (Figure 2A). The cluster comprises altogether six miRNAs, namely miR-106b-5p/-3p, miR-93-5p/-3p, and miR-25-3p/-5p, but only five of them were detected in endothelial cells with qPCR (Figure 2B). Of note, miR-25-5p was detected from endothelial cells with miRNA-seq, but its expression was too low for qPCR detection (i.e. Tags Per Million < 25) (Supplementary Table S3). Interestingly, oxPAPC treatment induced the cluster expression, but not the host gene expression (Figure 2C and Supplementary Figure S2A and B). To investigate the role of NRF2 in the upregulation of the cluster miRNAs, NRF2 inhibition approach was applied. NRF2 inhibition was achieved using two complementary methods: adenoviral overexpression of the NRF2 inhibitor, KEAP1 and NRF2 silencing. In basal state, NRF2 is tethered in the cytoplasm by two KEAP1 proteins, which work as adaptors

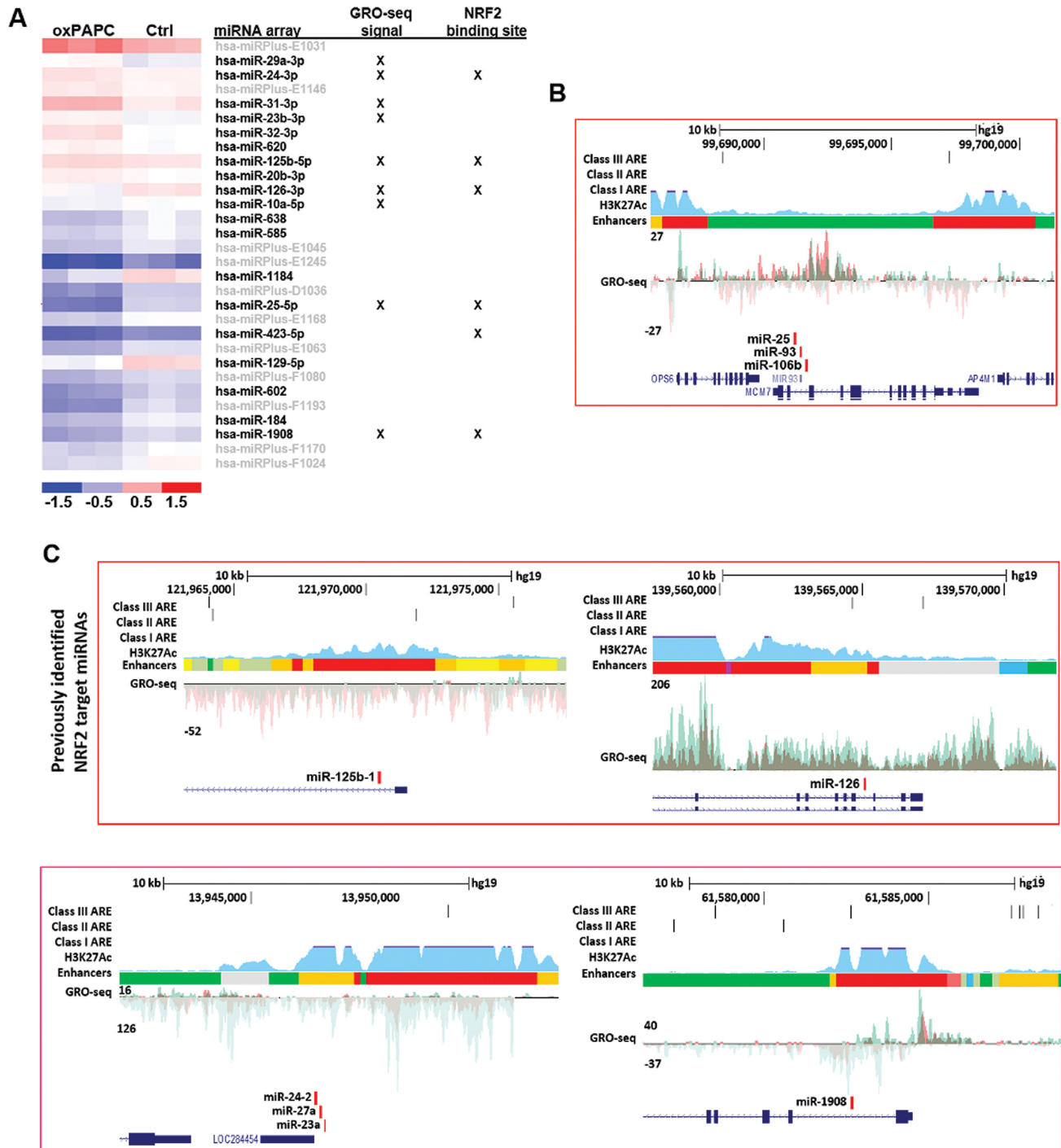


**Figure 1.** (A) miRNA array heatmap showing significantly altered miRNAs in response to oxPAPC treatment (4h) ( $P < 0.01$  two-tailed  $t$ -test). In addition, loci with confirmed GRO-seq signal and NRF2 binding sites on HUVEC enhancer/promoter elements  $\pm 5,000$  bp from miRNA/miRNA cluster locus are marked with 'X'. Predicted miRNAs are marked gray on the array, and discarded from further analysis. Color scale illustrates the relative expression level across all samples: red represents expression level above mean, blue expression lower than the mean. (B) *MIR25* loci showing NRF2 binding sites (antioxidant response elements, AREs), ENCODE H3K27Ac, ENCODE genome segmentation ('Enhancer') and GRO-seq signals in HUVECs. AREs are classified according to the estimated NRF2 binding as described in (15) (Class III-I: 'Medium' to 'Strong' binding sites). ENCODE H3K27Ac indicates active enhancers in HUVECs and ENCODE chromatin segmentation for HUVECs shows promoters in red, active enhancers in orange and active chromatin in green (47). The segmentation integrates ChIP-seq data for eight chromatin marks, RNA Polymerase II, CTCF transcription factor, and input samples. For GRO-seq, control treatment is shown in red and oxPAPC (6h) in cyan. Transcription from plus strand is shown above the axis and transcription from negative strand below the axis. (C) Loci, which passed the criteria in addition to *MIR25* locus. Previously characterized NRF2-regulated miRNAs are indicated.

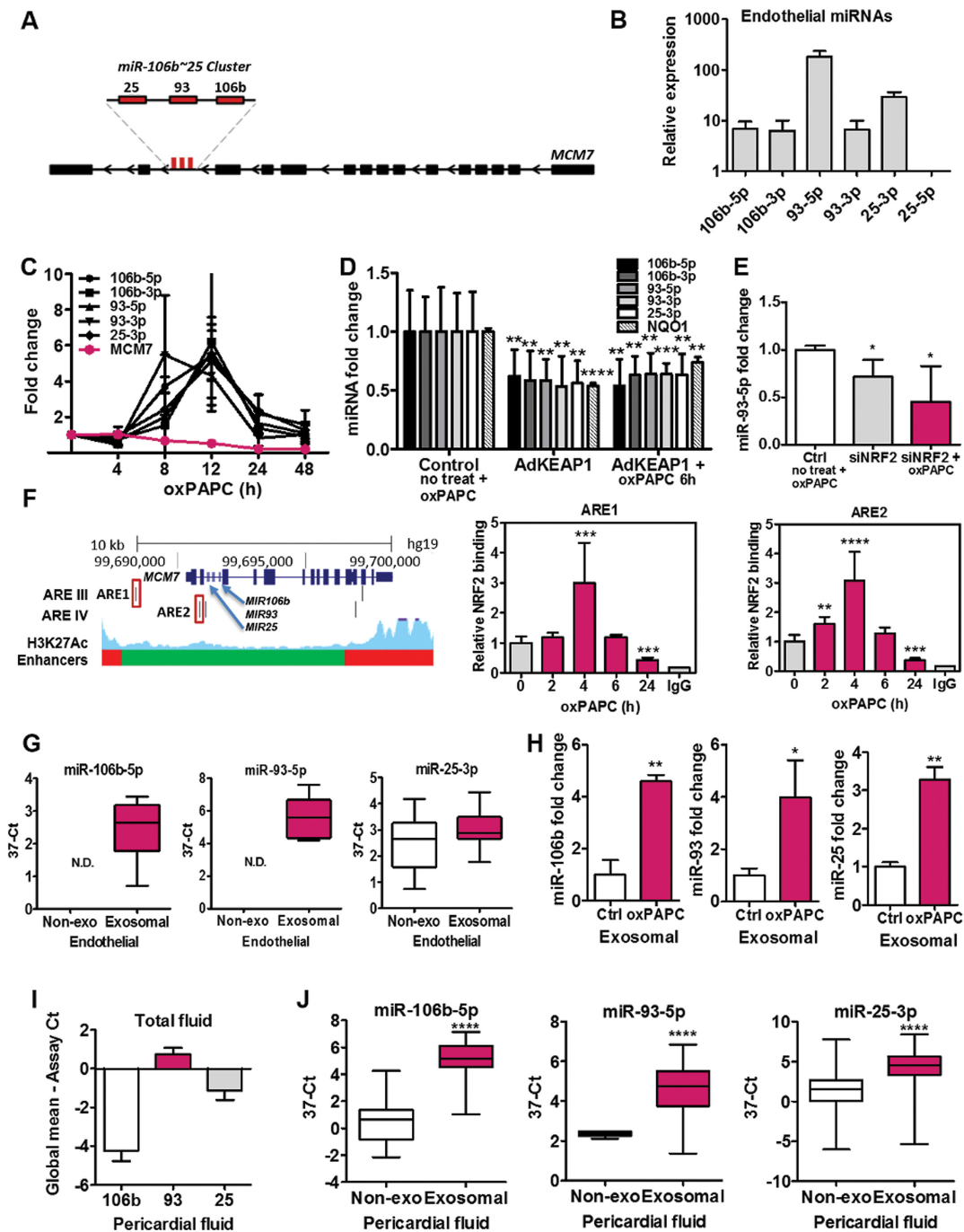


**Figure 2.** NRF2 regulates basal and oxPAPC-induced expression of miR-106b~25\*\*\* cluster. (A) *MCM7* gene and miR-106b~25 cluster. (B) Relative expression of miR-106b~25 cluster miRNAs in endothelial cells ( $n=36$ ). (C) Expression of miR-106b~25 cluster and its host gene, *MCM7*, in response to oxPAPC treatment. Fold change is calculated against respective control treatment in each time point ( $n=6$ ). (D) Expression of miR-106b~25 cluster miRNAs using adenoviral KEAP1 overexpression to inhibit NRF2 in oxPAPC-treated (6h,  $n=6$ ) and nontreated ( $n=9$ ) cells. Results were calculated as fold change against respective adenoviral controls. Control bar contains both oxPAPC-treated and nontreated control values. *NQO1* is shown as a positive control. (E) Expression of miR-93-5p in control siRNA and siNRF2 treated cells in basal and oxPAPC (8h) conditions ( $n=3$ ). The fold changes were calculated against respective controls. (F) Promoter/enhancer analysis of *MCM7* locus showing NRF2 binding sites (antioxidant response elements, AREs). The AREs are classified according to estimated NRF2 binding (Class III-IV: 'Medium' to 'Medium weak' binding sites (15)) ENCODE HUVEC H3K27Ac marks active enhancers and HUVEC chromatin segmentation shows promoters in red (dark gray) and active chromatin areas in green (light grey) (47). Selected AREs (ARE1 and ARE2) are highlighted. In the bar graphs, ChIP analysis of NRF2 binding on ARE1 and ARE2 in response to oxPAPC treatment is shown. Fold changes are calculated against respective control samples on each time point ( $n=3$ ). The values of all control samples are shown at 0. (G) miR-106b, miR-93 and miR-25 in exosome-depleted (non-exo) and exosomal fractions of endothelial growth medium ( $n=24$ , N.D. = not detected). (H) miRNAs in the endothelial exosomes of control and oxPAPC treated (12h) cells ( $n=3$ ). The results are calculated as fold change against control medium. (I) miRNAs in human pericardial fluid (total fluid values) ( $n=48$ ). Values were normalized to the global mean of all assays. (J) miRNAs in exosome-depleted (non-exo) and exosomal fractions of human pericardial fluid ( $n=48$ ) (for B–F, H–I: mean  $\pm$  SD; for G, J: whiskers mark the highest and lowest values. \* $P < 0.05$ , \*\* $P < 0.01$ , \*\*\* $P < 0.001$ , \*\*\*\* $P < 0.0001$ )

mediating proteasomal degradation of NRF2. Upon physiological stimulation, KEAP1 is modified, which allows *de novo* synthesized NRF2 to accumulate in the nucleus and the initiation of target gene transcription (35). NRF2 inhibition reduced miRNA levels significantly both without and with oxPAPC (Figure 2D and E, Supplementary Figure S2C and D). Again, the effect on the host gene did not resemble the effect on cluster miRNAs (Supplementary Figure S2E-F). Finally, NRF2 binding was confirmed on two enhancers with ChIP both in basal and induced states (Figure 2F and Supplementary Figure S2G). The binding was shown to decrease in KEAP1-overexpressing cells compared to control cells both in the basal state and with oxPAPC treatment (Supplementary Figure S2H). Taken together, the data shows that the cluster is regulated by NRF2 both in the basal and induced states. Based on their higher relative expression levels in endothelial cells, miR-106b-5p (miR-106b), miR-93-5p (miR-93), and miR-25-3p (miR-25) were selected for further studies.

### miR-106b~25 cluster miRNAs in coronary artery disease patients

Endothelial cells are a substantial source of extracellular miRNAs detected from pericardial fluid (36,37). miRNAs can be secreted from the cells in vesicular carriers, such as exosomes, or in complex with protein carriers. In order to investigate the secretion of the cluster miRNAs from endothelial cells, the extracellular miRNAs were measured from the conditioned growth medium in basal state and with oxPAPC treatment. miR-106b and miR-93 were detected only from the exosomal fraction of the endothelial growth medium, whereas miR-25 was detected from both exosomal and exosome-depleted fractions (Figure 2G). OxPAPC treatment increased the secretion of all three miRNAs (Figure 2H).

miR-106b~25 cluster has been previously suggested to be upregulated in the plasma samples of coronary artery disease (CAD) patients with vulnerable plaques, and the source of the miRNAs was postulated to be endothelial cell derived microparticles (38). Therefore, we next set out to determine the presence of miR-106b, miR-93 and miR-25 in the pericardial fluid of heart failure patients. The miRNA levels in total pericardial fluid were in line with the levels in endothelial cells, and miR-93 was shown to be the most abundant of the three (Figure 2I). Similar to cultured endothelial cells, miR-106b and miR-93 were primarily found from the exosomal fraction of the fluid, whereas miR-25 was detected from both exosomal and non-exosomal fractions (Figure 2J). When the samples were grouped according to the classified heart failure symptom severity of the patients at the time of sample collection, the exosomal miR-25 levels showed a significant increase at the onset of heart failure symptoms, whereas miR-106b and miR-93 patterns were more random (Supplementary Figure S3A). However, when the samples were divided to groups of CAD and control patients, significantly lower miR-106b and miR-93 levels were detected in CAD patients compared to control group and the trend for miR-25 was the same, although not statistically significant (Supplementary Figure S3B). When the CAD patients were further divided according to the severity

of their heart failure symptoms, all three miRNAs showed an increase towards more severe symptoms (Supplementary Figure S3C). Collectively, the data implies that the exosomal miR-106b~25 cluster miRNAs may have potential as biomarkers, but the validation warrants further studies with larger cohorts.

### miR-93 targets endothelial glycolysis and proliferation pathways

To get a broader view of the cluster function in endothelial cells, RNA-seq with miRNA overexpression and inhibition was performed. As the most abundant miRNA of the cluster, miR-93 was selected for the studies. Of note, the seed sequence of miR-106b is identical with miR-93. Ingenuity Pathway Analysis (IPA) of the overexpression data revealed several hits on cell growth related pathways, which collectively implied endothelial activation and angiogenic stimulation of the cells (Supplementary Table S4). In accordance with IPA results, cellular proliferation was found to be significantly induced with miR-93 overexpression compared to control treatment (Figure 3A). Since glycolysis is essential for endothelial proliferation and angiogenesis (39,40), we next measured glucose-induced glycolysis and maximal glycolytic capacity using the Seahorse flux analysis, and found both to be significantly increased in miR-93 overexpressing cells compared to control cells (Figure 3B).

To investigate the mechanisms through which miR-93 affects glycolysis, miR-93 overexpression datasets were compared to miR-93 inhibition data, and the putative target genes were listed (Supplementary Table S5). Among the most downregulated transcripts was *KLF2*, which has been shown to upregulate *PFKFB3*, a key regulator of glycolysis in endothelial cells (41). The RNA-seq signal for *KLF2* showed a significant decrease in response to miR-93 overexpression, and an increase to miR-93 inhibition compared to respective control signals (Figure 4A). These results were confirmed by qPCR measurements (Figure 4B, Supplementary Figure S4A). In addition, miR-93 overexpression reduced *KLF2* response to oxPAPC compared to control cells (Figure 4C, Supplementary Figure S4B), and miR-93 binding to *KLF2* mRNA was confirmed with a pull-down assay in endothelial cells (Figure 4D). Finally, *KLF2* silencing upregulated *PFKFB3*, and western blot analysis showed a mild decrease in *KLF2* and a slight increase in *PFKFB3* in miR-93 overexpressing cells compared to control cells (Figure 4E and F). Taken together, the data shows that miR-93 targets *KLF2*, which increases glycolysis rate through *PFKFB3*. However, miR-93 overexpression eventually affected *PFKFB3* mRNA levels as the cellular *KLF2* expression decreased and *PFKFB3* increased (Supplementary Figure S4C), and the biotin pulldown assay confirmed miR-93 binding to *PFKFB3* mRNA (Supplementary Figure S4D). Thus, depending on their relative expression levels, miR-93 targets either the inhibitor (*KLF2*) or the activator (*PFKFB3*) of glycolysis thereby either promoting or inhibiting endothelial activation.

Regarding proliferation, further analysis of the RNA-seq data revealed a significant activation of VEGFA and MYC pathways. In endothelial cells, VEGFA signalling is coupled to endothelial metabolism and proliferation through

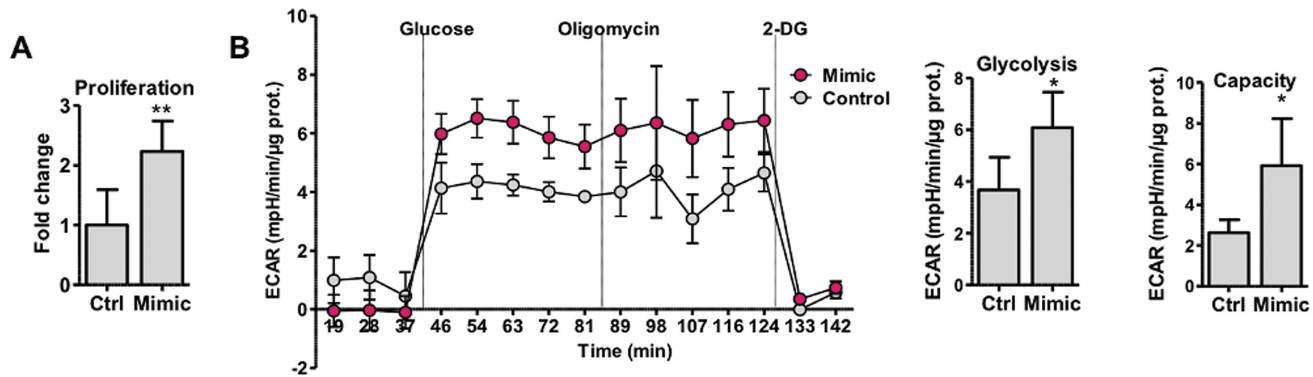


**Figure 3.** miR-93 controls endothelial proliferation and glycolysis. (A) Proliferation assay results in control and miR-93 overexpressing endothelial cells. Fold change is calculated against miRNA control cells (mean  $\pm$  SD,  $n=6$ ). (B) Glycolysis stress test results in miR-93 overexpressing and miRNA control cells (mean  $\pm$  SEM,  $n=5$ ). Glycolysis rate and glycolytic capacity of miR-93 overexpressing and miRNA control cells ( $n=5$ ) (mean  $\pm$  SD) (for all: \* $P < 0.05$ , \*\* $P < 0.01$ )

FOXO1 and MYC (42). Therefore, we next determined miR-93 effects on the VEGFA-FOXO1-MYC axis. In miR-93 overexpressing cells, *VEGFA* was found to be upregulated (Supplementary Figure S4E), and *FOXO1* mRNA was significantly downregulated compared to control cells, whereas FOXO1 protein was slightly upregulated with miR-93 inhibition compared to control cells (Figure 4G and H). FOXO1 was further validated to be a direct miR-93 target with the pulldown assay (Figure 4I). However, also MYC was found to be a direct miR-93 target (Supplementary Figure S4F and G) confirming a regulatory loop between FOXO1, MYC and miR-93. Collectively, the data shows that miR-93 controls glycolysis through KLF2 and PFKFB3, and proliferation through VEGFA, FOXO1 and MYC (Figure 4J).

### OxPAPC stimulates glycolysis and proliferation

Next, we set out to investigate whether the effects of oxPAPC were consistent with miR-93 effects on glycolysis and proliferation. In short, oxPAPC was shown to stimulate glycolysis through PFKFB3 (Figure 5A and B) and proliferation through VEGFA and MYC (Figure 5C–E). As NRF2 is a known mediator of oxPAPC effects (7) as well as a regulator of miR-93 expression, we postulated that NRF2 is the mediator of the stimulatory effects of oxPAPC on glycolysis and proliferation through transcriptional regulation of PFKFB3, VEGFA, FOXO1 and MYC (Figure 5F).

### NRF2 mediates the effects of oxPAPC and controls endothelial glycolysis, proliferation and quiescence

To confirm the regulatory role of NRF2 in glycolysis and proliferation, NRF2 silencing, overexpression and binding models (15) were utilized. First, oxPAPC effect on glycolysis and proliferation was shown to be reversed by NRF2 silencing (Figure 6A and B). In addition, NRF2 silencing reduced the expression of *PFKFB3*, *VEGFA* and *MYC*, and increased *FOXO1* in oxPAPC-treated cells (Supplementary Figure S5). NRF2 overexpression, on the other hand, was shown to increase glycolysis and proliferation (Figure 6C and D). NRF2 overexpression was also shown

to increase and silencing decrease PFKFB3 and MYC, whereas FOXO1 was downregulated by NRF2 overexpression and upregulated by NRF2 silencing (Figure 6E and G and Supplementary Figure S6A). In order to investigate the necessity of miR-93 for NRF2-driven facilitation of glycolysis, glycolysis rate was measured from NRF2- and miR-93-silenced cells. NRF2 inhibition was shown to decrease glycolysis in basal state, whereas miR-93 inhibition alone was not sufficient for reduction of glycolysis (Supplementary Figure S6B) thereby confirming that NRF2 is the main driver of the effect between the two. Furthermore, promoter/enhancer analyses revealed several putative NRF2 binding sites on the regulatory regions of *PFKFB3*, *VEGFA*, *FOXO1* and *MYC* (Supplementary Figure S7A) and, despite the previous reports stating that oxPAPC-induced VEGFA response is regulated by NRF2 through ATF4 (43), ChIP confirmed NRF2 binding to all selected locations and oxPAPC was shown to further increase the binding (Supplementary Figure S7B). Moreover, GRO-seq confirmed the transcriptional activation of *PFKFB3*, *VEGFA* and *MYC* loci and repression of *FOXO1* in response to oxPAPC treatment (Supplementary Figure S7A).

NRF2 and KLF2 are important regulators of endothelial function. Together they have been estimated to regulate approximately 70% of the shear stress responsive genes (44). Interestingly, in this study, KLF2 was shown to be oxPAPC-responsive (Figure 6H and I). Therefore, we postulated that KLF2 expression could also be regulated by NRF2. Indeed, promoter analysis revealed several putative NRF2 binding sites residing on both KLF2 promoter and enhancer areas in endothelial cells and GRO-seq signal confirmed strong transcriptional activation in response to oxPAPC treatment (Supplementary Figure S8A). The binding of NRF2 to the response elements was verified with ChIP and shown to increase in response to oxPAPC treatment (Supplementary Figure S8B). Moreover, NRF2 overexpression increased and silencing decreased KLF2 expression both in basal state and with oxPAPC treatment (Figure 6H and I). Together, these results show that NRF2 controls endothelial glycolysis and proliferation through transcrip-

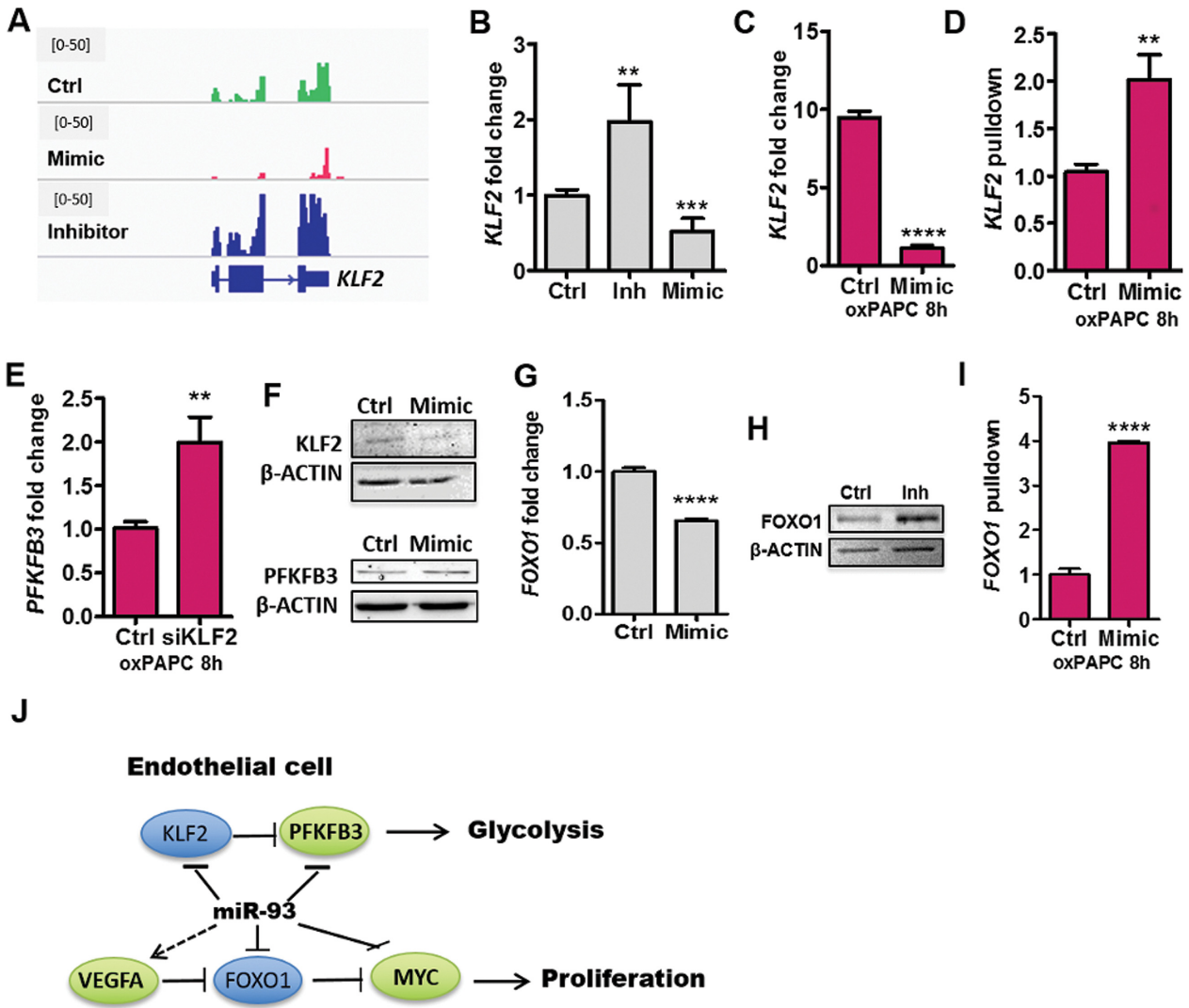


**Figure 4.** miR-93 controls glycolysis through *KLF2* and *PFKFB3* regulation, and proliferation through *VEGFA*, *FOXO1* and *MYC*. (A) IGV (32) snapshot for RNA-seq signal of *KLF2* locus. Representative tracks are shown. (B) *KLF2* expression in miRNA control, miR-93-inhibited (inh) and overexpressing (mimic) cells. Fold changes are calculated against respective controls and both mimic and inhibitor control values are combined to ‘ctrl’ bar ( $n=6$ ). (C) *KLF2* expression in miRNA control and miR-93 overexpressing cells with oxPAPC treatment (8h). Fold changes are calculated against miRNA control in control conditions (i.e. oxPAPC control treatment) ( $n=3$ ). (D) Enrichment of *KLF2* mRNA in pull-down samples using transfected biotinylated control miRNA (cel-miR-39-3p) and biotinylated miR-93 mimic in oxPAPC-treated (8h) endothelial cells. Fold change is calculated against control miRNA values ( $n=3$ ). (E) *PFKFB3* expression in siRNA control and siKLF2 cells with oxPAPC treatment (8h). (F) Representative Western blots for *KLF2* and *PFKFB3* in miRNA control and miR-93 overexpressing endothelial cells. Fold change is calculated against mimic control ( $n=6$ ). (G) *FOXO1* expression in miRNA control and miR-93 overexpressing cells. Fold change is calculated against control miRNA values ( $n=3$ ). (H) A representative Western blot for *FOXO1* in miRNA control and miR-93-silenced cells. (I) Amount of *FOXO1* mRNA in pull-down samples of control miRNA (cel-miR-39-3p) and biotinylated miR-93 mimic in oxPAPC-treated (8h) endothelial cells. Fold change is calculated against control miRNA values ( $n=3$ ). (J) Mechanistic overview of the findings (for all: mean  $\pm$  SD, \*\* $P < 0.01$ , \*\*\* $P < 0.001$ , \*\*\*\* $P < 0.0001$ )

tional regulation of *PFKFB3*, *VEGFA*, *FOXO1* and *MYC*, and quiescence through *KLF2* (Figure 6J).

### DISCUSSION

Vascular endothelium forms the inner lining of the heart and blood vessels. It functions as a selective barrier between the vessel lumen and the surrounding tissue allowing the exchange of nutrients and gases between the blood and tissues. However, vascular endothelium is not just a passive barrier, it actively secretes signals that modify its own and neighboring cell and tissue function. In adult blood vessels, endothelial cells resume quiescence, which is a reversible state char-

acterized by non-dividing and non-migratory cellular phenotype. Quiescent endothelium can be evoked to establish new vascular networks to relieve local nutrient and oxygen deprivation or by substances that stimulate neovascularisation, such as oxidized phospholipids (9,45). In this study, we have characterized novel mechanisms through which oxidized phospholipids of oxPAPC affect endothelial function, and the role of miR-93 and NRF2 in the process.

miRNA expression is controlled by epigenetic mechanisms that control the accessibility of the genomic region and transcription factors, which recruit or inhibit the recruitment of the transcriptional machinery. In humans, the

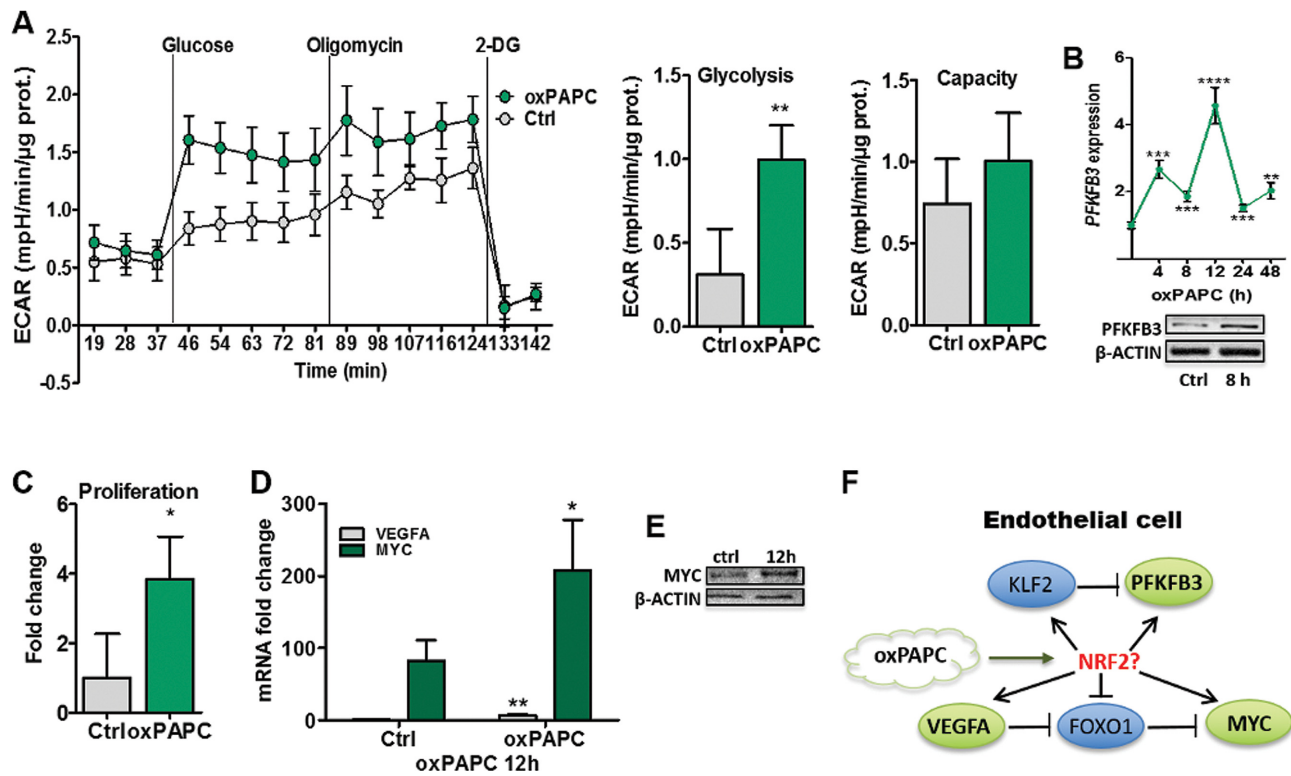


**Figure 5.** NRF2 mediates the effects of oxPAPC on glycolysis and proliferation. (A) Glycolysis stress test (mean  $\pm$  SEM,  $n=5$ ), glycolytic rate (mean  $\pm$  SD,  $n=5$ ) and glycolytic capacity (mean  $\pm$  SD,  $n=5$ ) in oxPAPC and control treated endothelial cells. (B) *PFKFB3* expression in oxPAPC-treated cells and representative Western blot of *PFKFB3* of oxPAPC (8h) and control treated cells. Fold changes are calculated against respective control treatments in each time point ( $n=6$ ). (C) Proliferation assay for control and oxPAPC-treated cells. Fold change is calculated against control cells ( $n=6$ ). (D) Expression of *VEGFA* and *MYC* in control and oxPAPC treated (12h) cells. Fold changes are calculated against *VEGFA* control values ( $n=3$ ). (E) Representative Western blot for *MYC* in control and oxPAPC treated (12h) cells. (F) Overview of the suggested mechanism (for B-D: mean  $\pm$  SD, \* $P < 0.05$ , \*\* $P < 0.01$ , \*\*\* $P < 0.001$ , \*\*\*\* $P < 0.0001$ ).

majority of miRNAs are located in the intronic or intergenic regions, but they can also be encoded from exons (46). Intronic miRNA may share a common promoter with its host gene or can be expressed independently through its own promoter, as demonstrated here for the miR-106b~25 cluster and its host gene *MCM7*. For most miRNA genes, the precise locations of their promoters are unknown, but can be estimated from the next generation sequencing data, such as GRO-seq and ChIP-seq data. More recently, a DROSHA-knockout cell approach was reported of being applied to map human miRNA promoters (18). The study reported a significant enrichment of NRF2 binding sites in the mapped promoters suggesting NRF2 to be a common regulator of miRNA expression. However, transcriptional regulators of miRNA expression are in general poorly characterized. In this study, the combination of GRO-seq and miRNA array data was utilized to gain a set of oxPAPC-responsive miRNAs in HUVECs. The selection was further filtered to contain only putative NRF2-regulated miRNAs using a previously established genome-wide NRF2 binding model (15) together with ENCODE data for active enhancers in HUVECs (47). The approach resulted in five candidate miRNA loci. In addition to the miR-106b~25 cluster, which was characterized here, two of the loci had been previously shown to be NRF2 regulated. The NRF2 binding model was also utilized to resolve the underlying

mechanisms for the NRF2-mediated oxPAPC-response in endothelial cells. Thus, combining the model with next generation sequencing data has proven to be a successful approach for characterizing novel NRF2-regulated noncoding RNAs and target genes.

A Recent study by Ren *et al.* identified a distinct miRNA profile for patients with unstable plaques, which set them aside from the patients with stable coronary artery disease (CAD) (38). One of the upregulated clusters in vulnerable CAD was miR-106b~25, and the source of upregulated miRNAs was reported to be CD31+/Annexin V+ microparticles (MPs). CD31+/Annexin V+ MPs have been shown to originate from endothelial cells and platelets and to correlate with impairment of coronary endothelial function (38,48). Moreover, high levels of circulating CD31+/Annexin V+ MPs are associated with higher risk of cardiovascular death (49). In this study, exosomal miRNA levels of miR-106b, miR-93 and miR-25 were shown to be lower in CAD patients compared to control group, but to increase with CAD progression. Most variable values were detected in the group of patients with severe heart failure symptoms dividing the group into subgroups of very low and very high values, which could potentially arise from patients with stable and vulnerable CAD, respectively. Although our results originate from a relatively small patient population, together with recent studies, they support the

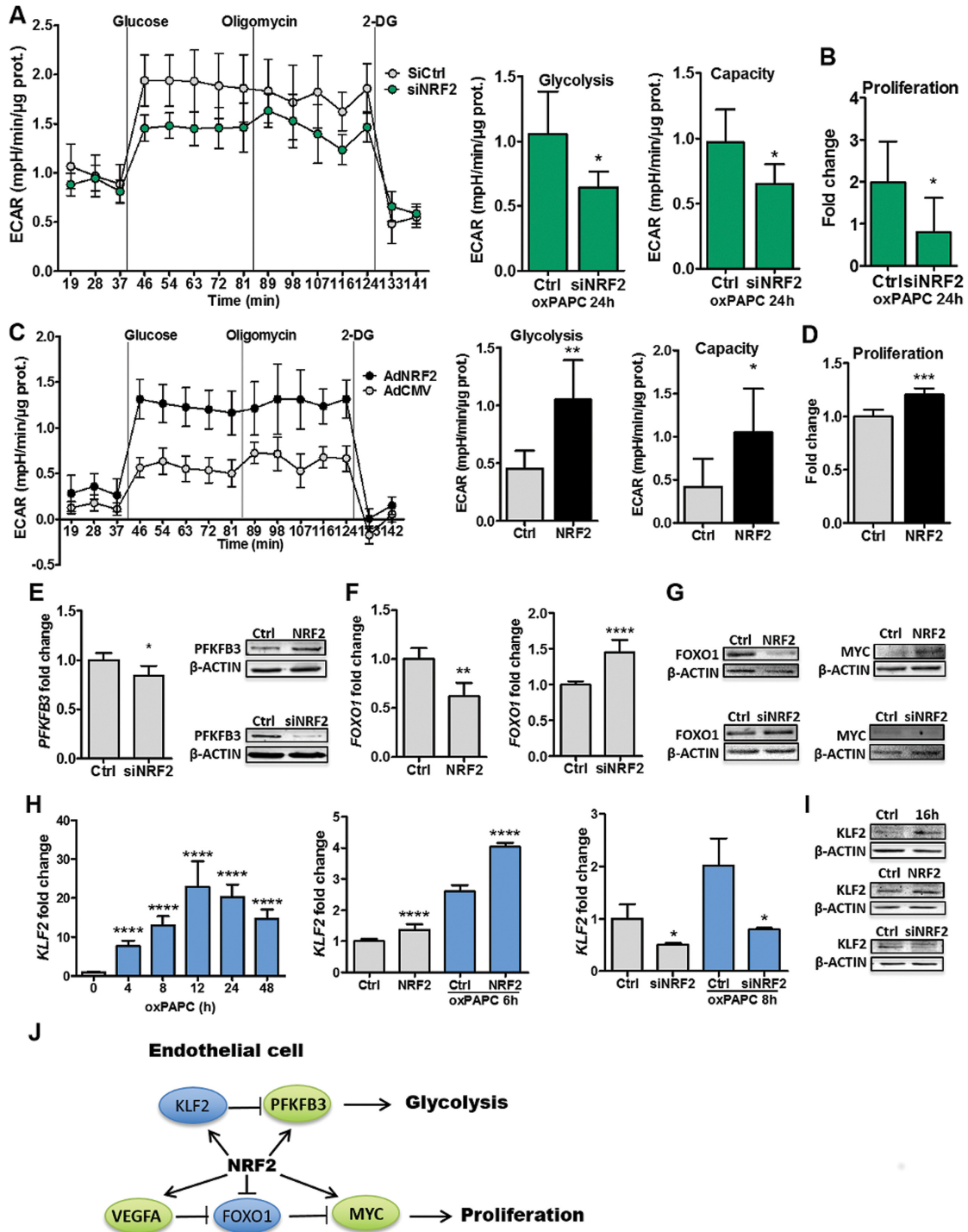


**Figure 6.** NRF2 regulates glycolysis and proliferation through transcriptional regulation of KLF2, PFKFB3, VEGFA, FOXO1 and MYC. (A) Glycolysis stress test (mean ± SEM,  $n=5$ ), glycolytic rate (mean ± SD,  $n=5$ ) and glycolytic capacity (mean ± SD,  $n=5$ ) in control siRNA and siNRF2 transfected oxPAPC treated (24h) endothelial cells. (B) Proliferation assay for siRNA control and NRF2-silenced cells. Fold change is calculated against control cells ( $n=6$ ). (C) Glycolysis stress test in adenoviral NRF2-overexpressing and control-transduced endothelial cells (mean ± SEM,  $n=5$ ). Glycolysis rate and glycolytic capacity of endothelial cells transduced with adenoviral NRF2-overexpressing or control vectors or control cells (mean ± SD,  $n=5$ ). (D) Proliferation assay for NRF2-overexpressing and control transduced cells. Fold change is calculated against control cells ( $n=6$ ). (E) Expression of *PFKFB3* in siRNA control or siNRF2 transfected cells. Fold change is calculated against siRNA control ( $n=6$ ). Representative Western blots for *PFKFB3* in NRF2-overexpressing and NRF2-silenced endothelial cells with respective controls. (F) *FOXO1* expression in NRF2-overexpressing and NRF2-silenced endothelial cells. Fold changes are calculated against respective controls ( $n=6$ ). (G) Representative Western blots for *FOXO1* and *MYC* with NRF2 overexpression, NRF2 silencing and their respective controls. (H) *KLF2* expression in oxPAPC-treated, NRF2-overexpressing, and NRF2-silenced cells. Fold changes are calculated against respective nontreated control values (oxPAPC:  $n=3$ ; NRF2-oe:  $n=9$  for nontreated,  $n=6$  for oxPAPC; siNRF2:  $n=3$ ). (I) Representative western blots for *KLF2* in oxPAPC-treated (16h), NRF2-overexpressing and siNRF2 cells with respective controls. (J) Mechanistic overview of the findings (for B, D–F, H; mean ± SD, \* $P < 0.05$ , \*\* $P < 0.01$ , \*\*\* $P < 0.001$ , \*\*\*\* $P < 0.0001$ ).

diagnostic and prognostic potential of vesicular miRNAs. Furthermore, all three miRNAs were shown to respond to oxPAPC treatment, which increased both their expression and secretion. Collectively, these findings suggest accumulation of the miRNAs in endothelial cells of atherosclerotic plaques, which, in turn, could contribute to the increased release of miRNA containing vesicles (38). However, the miRNA expression patterns in endothelial cells of atherosclerotic lesions are not known, although a recent study by Raitoharju *et al.* (50) showed a mild, albeit not statistically significant, increase of miR-106b, miR-93 and miR-25 in human aortic atherosclerotic plaques compared to control samples.

In general, miRNAs function by exerting modest inhibitory effects on multiple targets of the same biological process (51). Their typical targets are transcription factors, especially those that control their own expression. miR-93 has been previously shown to target NRF2 (52), whereas MYC has been shown to regulate miR-93 expression (53). Here, NRF2 was shown to control the expression of both miR-93 and MYC, whereas miR-93 was shown to target MYC. miRNAs may also target both positive and negative regulators of the same biological process, which allows buffering against minor shifts in activity and may help to restore basal status after activating stimuli recedes (51). In this study, miR-93 was identified to target both KLF2 and PFKFB3, which act as inhibitor and stimulator of glycolysis, respectively, as well as to target FOXO1 and MYC, which have opposing effects on cellular proliferation (39,41,54).

Endothelial cell function relies on glycolysis and is dependent on constant glucose flux, so much so that glucose starvation is cytotoxic (55). Like cancer cells, endothelial cells generate up to 85% of their ATP through glycolysis, and the rate is further increased by twofold when the cells shift from quiescence to proliferation (39,40). Endothelial quiescence is maintained through atheroprotective KLF2 function, which represses PFKFB3 (12). PFKFB3, an activator of a key glycolytic enzyme, 6-phosphofructo-1-kinase (PFK-1), has been shown to be a critical factor in the glycolytic regulation of endothelial proliferation and angiogenesis. Inhibition of PFKFB3 reduces endothelial cell glycolysis by 30–40%, which is sufficient to reduce proliferation significantly and impair angiogenesis (39,40). FOXO1, on the other hand, couples VEGFA signalling to endothelial metabolism and proliferation (42). FOXO1 is the gatekeeper of endothelial quiescence reducing glycolysis and proliferation through suppression of MYC, which in turn is the master regulator of anabolic metabolism and growth (54). Inhibition of FOXO1 or activation of MYC signalling restores proliferative phenotype and promotes angiogenesis (54,56,57). In this study, NRF2 was found to control endothelial activity and to mediate the effects of oxPAPC through transcriptional regulation of PFKFB3, VEGFA, FOXO1, MYC and KLF2. Collectively, the control of the multifaceted regulatory network allows NRF2 and miR-93 to switch the phenotype from quiescent to proliferative and back depending on the environmental cues.

Consistent with our findings, miR-93 overexpression has been previously shown to promote angiogenesis both *in vitro* and *in vivo*, as well as healthy neovessel formation

in tumour microenvironment (58,59). Previous studies have also shown NRF2 to be critical for physiological angiogenesis and neovascularisation both *in vitro* and *in vivo*, but the mechanism has remained unclear (60,61). Although oxPAPC has been previously demonstrated to stimulate angiogenesis (6) the regulatory interplay of oxPAPC, NRF2 and miR-93 in the process has not been shown before. Here, NRF2 was not only shown to control the expression of the critical angiogenic factors, but also to mediate oxPAPC effect on endothelial activation. In addition, NRF2 was shown to control miR-106b~25 cluster expression in the basal state and to mediate the oxPAPC-response of the cluster.

The ability of individual miRNAs to target hundreds of different RNA molecules makes them attractive drug candidates and targets for complex diseases like atherosclerosis and cancer, which involve many pathways and would likely benefit from multifaceted therapeutics (62). However, many features of miRNA biology are still unknown, and the exploration of miRNA function is at an early stage of discovery. Here, we have established several novel regulatory loops between NRF2, miR-93 and the essential regulators of healthy endothelium. Collectively, the data shows that NRF2 controls the switch between active and quiescent endothelial states together with miR-93, and provides a novel mechanism through which oxidized phospholipids evoke the quiescent endothelium.

## AVAILABILITY

RNA-seq data has been deposited in the Gene Expression Omnibus (GEO) (63) under accession number GSE86497. GEO accession number is GSE102501 for the endothelial miRNA array, GSE103530 for the GRO-seq data, GSE94410 for the miRNA-seq, and GSM733691 for the H3K27Ac dataset. UCSC Accession for the ChromHMM segmentation is wgEncodeAwgSegmentationChromhmmHuvec.

## SUPPLEMENTARY DATA

Supplementary Data are available at NAR online.

## ACKNOWLEDGEMENTS

We thank Mrs Arja Korhonen for outstanding technical assistance, Dr Ken Itoh for Keap1 antibody and Dr Aikseng Ooi for bioinformatics training.

## FUNDING

Instrufoundation (to S.M.K.); Finnish Cultural Foundation, North Savo Regional Fund (to S.M.K.); Emil Aaltonen Foundation (to S.M.K. and E.K.); Finnish Foundation for Cardiovascular Research (to S.M.K. and M.U.K.); Aarne and Aili Turunen Foundation (to S.M.K.); Maud Kuistila Memorial Foundation (to S.M.K.); Antti and Tyne Soinen Foundation (to S.M.K.); Aarne Koskelo Foundation (to S.M.K.); Saara Kuusisto and Salme Penanen Foundation (to S.M.K.); Ida Montin Foundation (to S.M.K.); Kuopio University Foundation (to S.M.K.);

Orion-Farmos Research Foundation (to E.K.); Finnish Funding Agency for Technology and Innovation (to P.Ta.); European Regional Development Fund (to P.Ta.); Sigrid Juselius Foundation (to M.U.K. and A-L.L.); Jane and Aatos Erkko Foundation (to M.U.K. and A-L.L.); Finnish Cancer Foundation (to A-L.L.); Academy of Finland [287478 to M.U.K. and 275147 to A-L.L.]. Funding for open access charge: the Academy of Finland.  
*Conflict of interest statement.* None declared.

## REFERENCES

- Chiu, J.-J. and Chien, S. (2011) Effects of disturbed flow on vascular endothelium: pathophysiological basis and clinical perspectives. *Physiol. Rev.*, **91**, 327–387.
- Camaré, C., Pucelle, M., Nègre-Salvayre, A. and Salvayre, R. (2017) Angiogenesis in the atherosclerotic plaque. *Redox Biol.*, **12**, 18–34.
- Hayes, J.D. and Dinkova-Kostova, A.T. (2014) The Nrf2 regulatory network provides an interface between redox and intermediary metabolism. *Trends Biochem. Sci.*, **39**, 199–218.
- Lee, S., Birukov, K.G., Romanoski, C.E., Springstead, J.R., Lusa, A.J. and Berliner, J.A. (2012) Role of phospholipid oxidation products in atherosclerosis. *Circ. Res.*, **111**, 778–799.
- Watson, A.D., Leitinger, N., Navab, M., Faull, K.F., Hörkkö, S., Witztum, J.L., Palinski, W., Schwenke, D., Salomon, R.G., Sha, W. *et al.* (1997) Structural identification by mass spectrometry of oxidized phospholipids in minimally oxidized low density lipoprotein that induce monocyte/endothelial interactions and evidence for their presence in vivo. *J. Biol. Chem.*, **272**, 13597–13607.
- Bochkov, V.N., Philippova, M., Oskolkova, O., Kadl, A., Furnkranz, A., Karabeg, E., Afonyushkin, T., Gruber, F., Breuss, J., Minchenko, A. *et al.* (2006) Oxidized phospholipids stimulate angiogenesis via autocrine mechanisms, implicating a novel role for lipid oxidation in the evolution of atherosclerotic lesions. *Circ. Res.*, **99**, 900–908.
- Jyrkkänen, H.-K., Kansanen, E., Inkala, M., Kivela, A.M., Hurttala, H., Heinonen, S.E., Goldsteins, G., Jauhiainen, S., Tiainen, S., Makkonen, H. *et al.* (2008) Nrf2 regulates antioxidant gene expression evoked by oxidized phospholipids in endothelial cells and murine arteries in vivo. *Circ. Res.*, **103**, e1–e9.
- Ke, Y., Zebda, N., Oskokova, O., Afonyushkin, T., Berdyshev, E., Tian, Y., Meng, F., Sarich, N., Bochkov, V.N., Wang, J.M. *et al.* (2017) Anti-inflammatory effects of OxPAPC involve endothelial cell mediated generation of LXA4. *Circ. Res.*, **121**, 244–257.
- Bochkov, V.N., Oskolkova, O.V., Birukov, K.G., Levenon, A.-L., Binder, C.J. and Stöckl, J. (2010) Generation and biological activities of oxidized phospholipids. *Antioxid. Redox Signal.*, **12**, 1009–1059.
- Sihvola, V. and Levenon, A.-L. (2017) Keap1 as the redox sensor of the antioxidant response. *Arch. Biochem. Biophys.*, **617**, 94–100.
- Andreou, I., Sun, X., Stone, P.H., Edelman, E.R. and Feinberg, M.W. (2015) miRNAs in atherosclerotic plaque initiation, progression, and rupture. *Trends Mol. Med.*, **21**, 307–318.
- Schober, A., Nazari-Jahantigh, M. and Weber, C. (2015) MicroRNA-mediated mechanisms of the cellular stress response in atherosclerosis. *Nat. Rev. Cardiol.*, **12**, 361–374.
- Schrottmaier, W.C., Oskolkova, O.V., Schabbauer, G. and Afonyushkin, T. (2014) MicroRNA miR-320a modulates induction of HO-1, GCLM and OKL38 by oxidized phospholipids in endothelial cells. *Atherosclerosis*, **235**, 1–8.
- Afonyushkin, T., Oskolkova, O.V. and Bochkov, V.N. (2012) Permissive role of miR-663 in induction of VEGF and activation of the ATF4 branch of unfolded protein response in endothelial cells by oxidized phospholipids. *Atherosclerosis*, **225**, 50–55.
- Kuosmanen, S.M., Viitala, S., Laitinen, T., Peräkylä, M., Pölönen, P., Kansanen, E., Leinonen, H., Raju, S., Wienecke-Baldacchino, A., Näränen, A. *et al.* (2016) The effects of sequence variation on genome-wide NRF2 binding-new target genes and regulatory SNPs. *Nucleic Acids Res.*, **44**, 1760–1775.
- Das, S. and Halushka, M.K. (2015) Extracellular vesicle microRNA transfer in cardiovascular disease. *Cardiovasc. Pathol.*, **24**, 199–206.
- Njock, M.-S. and Fish, J.E. (2017) Endothelial miRNAs as cellular messengers in cardiometabolic diseases. *Trends Endocrinol. Metab.*, **28**, 237–246.
- Jeong, G., Lim, Y.-H. and Kim, Y.-K. (2016) Precise mapping of the transcription start sites of human microRNAs using DROSHA knockout cells. *BMC Genomics*, **17**, 908.
- Ritchie, M.E., Silver, J., Oshlack, A., Holmes, M., Diyagama, D., Holloway, A. and Smyth, G.K. (2007) A comparison of background correction methods for two-colour microarrays. *Bioinformatics*, **23**, 2700–2707.
- Bouvy-Liivrand, M., Hernández de Sande, A., Pölönen, P., Mehtonen, J., Vuorenmaa, T., Niskanen, H., Sinkkonen, L., Kaikkonen, M.U. and Heinäniemi, M. (2017) Analysis of primary microRNA loci from nascent transcriptomes reveals regulatory domains governed by chromatin architecture. *Nucleic Acids Res.*, **23**, 862–876.
- Kaikkonen, M.U., Niskanen, H., Romanoski, C.E., Kansanen, E., Kivela, A.M., Laitalainen, J., Heinz, S., Benner, C., Glass, C.K. and Ylä-Herttuala, S. (2014) Control of VEGF-A transcriptional programs by pausing and genomic compartmentalization. *Nucleic Acids Res.*, **42**, 12570–12584.
- Kuosmanen, S.M., Kansanen, E., Sihvola, V. and Levenon, A.-L. (2017) MicroRNA profiling reveals distinct profiles for tissue-derived and cultured endothelial cells. *Sci. Rep.*, **7**, 10943.
- Kozomara, A. and Griffiths-Jones, S. (2014) miRBase: annotating high confidence microRNAs using deep sequencing data. *Nucleic Acids Res.*, **42**, D68–D73.
- Langmead, B. and Salzberg, S.L. (2012) Fast gapped-read alignment with Bowtie 2. *Nat. Methods*, **9**, 357–359.
- Robinson, M.D., McCarthy, D.J. and Smyth, G.K. (2010) edgeR: a Bioconductor package for differential expression analysis of digital gene expression data. *Bioinformatics*, **26**, 139–140.
- McCarthy, D.J., Chen, Y. and Smyth, G.K. (2012) Differential expression analysis of multifactor RNA-Seq experiments with respect to biological variation. *Nucleic Acids Res.*, **40**, 4288–4297.
- Kozarsky, K.F. and Wilson, J.M. (1993) Gene therapy: adenovirus vectors. *Curr. Opin. Genet. Dev.*, **3**, 499–503.
- Levenon, A.-L., Inkala, M., Heikura, T., Jauhiainen, S., Jyrkkänen, H.-K., Kansanen, E., Määttä, K., Romppanen, E., Turunen, P., Rutanen, J. *et al.* (2007) Nrf2 gene transfer induces antioxidant enzymes and suppresses smooth muscle cell growth in vitro and reduces oxidative stress in rabbit aorta in vivo. *Arterioscler. Thromb. Vasc. Biol.*, **27**, 741–747.
- Wang, D., Garcia-Bassets, I., Benner, C., Li, W., Su, X., Zhou, Y., Qiu, J., Liu, W., Kaikkonen, M.U., Ohgi, K.A. *et al.* (2011) Reprogramming transcription by distinct classes of enhancers functionally defined by eRNA. *Nature*, **474**, 390–394.
- Kim, D., Pertea, G., Trapnell, C., Pimentel, H., Kelley, R. and Salzberg, S.L. (2013) TopHat2: accurate alignment of transcriptomes in the presence of insertions, deletions and gene fusions. *Genome Biol.*, **14**, R36.
- Robinson, J.T., Thorvaldsdóttir, H., Winckler, W., Guttman, M., Lander, E.S., Getz, G. and Mesirov, J.P. (2011) Integrative genomics viewer. *Nat. Biotechnol.*, **29**, 24–26.
- Thorvaldsdóttir, H., Robinson, J.T. and Mesirov, J.P. (2013) Integrative Genomics Viewer (IGV): high-performance genomics data visualization and exploration. *Brief. Bioinform.*, **14**, 178–192.
- Love, M.I., Huber, W. and Anders, S. (2014) Moderated estimation of fold change and dispersion for RNA-seq data with DESeq2. *Genome Biol.*, **15**, 550.
- Shah, N.M., Zaitseva, L., Bowles, K.M., MacEwan, D.J. and Rushworth, S.A. (2015) NRF2-driven miR-125B1 and miR-29B1 transcriptional regulation controls a novel anti-apoptotic miRNA regulatory network for AML survival. *Cell Death Differ.*, **22**, 654–664.
- Kansanen, E., Kuosmanen, S.M., Leinonen, H. and Levenon, A.-L. (2013) The Keap1-Nrf2 pathway: Mechanisms of activation and dysregulation in cancer. *Redox Biol.*, **1**, 45–49.
- Kuosmanen, S.M., Hartikainen, J., Hippeläinen, M., Kokki, H., Levenon, A.-L. and Tavi, P. (2015) MicroRNA profiling of pericardial fluid samples from patients with heart failure. *PLoS One*, **10**, e0119646.
- Beltrami, C., Besnier, M., Shantikumar, S., Shearn, A.I.U., Rajakaruna, C., Laftah, A., Sessa, F., Spinetti, G., Petretto, E., Angelini, G.D. *et al.* (2017) Human pericardial fluid contains exosomes enriched with cardiovascular-expressed microRNAs and promotes therapeutic angiogenesis. *Mol. Ther.*, **25**, 679–693.

38. Ren, J., Zhang, J., Xu, N., Han, G., Geng, Q., Song, J., Li, S., Zhao, J. and Chen, H. (2013) Signature of circulating microRNAs as potential biomarkers in vulnerable coronary artery disease. *PLoS One*, **8**, e80738.
39. De Bock, K., Georgiadou, M., Schoors, S., Kuchnio, A., Wong, B.W., Cantelmo, A.R., Quaegebeur, A., Ghesquière, B., Cauwenberghs, S., Eelen, G. *et al.* (2013) Role of PFKFB3-driven glycolysis in vessel sprouting. *Cell*, **154**, 651–663.
40. Schoors, S., De Bock, K., Cantelmo, A.R., Georgiadou, M., Ghesquière, B., Cauwenberghs, S., Kuchnio, A., Wong, B.W., Quaegebeur, A., Gouveia, J. *et al.* (2014) Partial and transient reduction of glycolysis by PFKFB3 blockade reduces pathological angiogenesis. *Cell Metab.*, **19**, 37–48.
41. Doddaballapur, A., Michalik, K.M., Manavski, Y., Lucas, T., Houtkooper, R.H., You, X., Chen, W., Zeiher, A.M., Potente, M., Dimmeler, S. *et al.* (2015) Laminar shear stress inhibits endothelial cell metabolism via KLF2-mediated repression of PFKFB3. *Arterioscler. Thromb. Vasc. Biol.*, **35**, 137–145.
42. Betsholtz, C. (2016) Vascular biology: transcriptional control of endothelial energy. *Nature*, **529**, 160–161.
43. Afonyushkin, T., Oskolkova, O.V., Philippova, M., Resink, T.J., Erne, P., Binder, B.R. and Bochkov, V.N. (2010) Oxidized phospholipids regulate expression of ATF4 and VEGF in endothelial cells via NRF2-dependent mechanism: novel point of convergence between electrophilic and unfolded protein stress pathways. *Arterioscler. Thromb. Vasc. Biol.*, **30**, 1007–1013.
44. Boon, R.A. and Horrevoets, A.J.G. (2009) Key transcriptional regulators of the vasoprotective effects of shear stress. *Hamostaseologie*, **29**, 39–43.
45. Potente, M. and Mäkinen, T. (2017) Vascular heterogeneity and specialization in development and disease. *Nat. Rev. Mol. Cell Biol.*, **18**, 477–494.
46. Ha, M. and Kim, V.N. (2014) Regulation of microRNA biogenesis. *Nat. Rev. Mol. Cell Biol.*, **15**, 509–524.
47. ENCODE Project Consortium, Bernstein, B.E., Birney, E., Dunham, I., Green, E.D., Gunter, C. and Snyder, M. (2012) An integrated encyclopedia of DNA elements in the human genome. *Nature*, **489**, 57–74.
48. Werner, N., Wassmann, S., Ahlers, P., Kosiol, S. and Nickenig, G. (2006) Circulating CD31+/Annexin V+ apoptotic microparticles correlate with coronary endothelial function in patients with coronary artery disease. *Arterioscler. Thromb. Vasc. Biol.*, **26**, 112–116.
49. Sinning, J.-M., Losch, J., Walenta, K., Böhm, M., Nickenig, G. and Werner, N. (2011) Circulating CD31+/Annexin V+ microparticles correlate with cardiovascular outcomes. *Eur. Heart J.*, **32**, 2034–2041.
50. Raitoharju, E., Lyytikäinen, L.-P., Levula, M., Oksala, N., Mennander, A., Tarkka, M., Klopp, N., Illig, T., Kähönen, M., Karhunen, P.J. *et al.* (2011) miR-21, miR-210, miR-34a, and miR-146a/b are up-regulated in human atherosclerotic plaques in the Tampere Vascular Study. *Atherosclerosis*, **219**, 211–217.
51. Small, E.M. and Olson, E.N. (2011) Pervasive roles of microRNAs in cardiovascular biology. *Nature*, **469**, 336–342.
52. Singh, B., Ronghe, A.M., Chatterjee, A., Bhat, N.K. and Bhat, H.K. (2013) MicroRNA-93 regulates NRF2 expression and is associated with breast carcinogenesis. *Carcinogenesis*, **34**, 1165–1172.
53. Zhao, Z.-N., Bai, J.-X., Zhou, Q., Yan, B., Qin, W.-W., Jia, L.-T., Meng, Y.-L., Jin, B.-Q., Yao, L.-B., Wang, T. *et al.* (2012) TSA suppresses miR-106b-93-25 cluster expression through downregulation of MYC and inhibits proliferation and induces apoptosis in human EMC. *PLoS One*, **7**, e45133.
54. Wilhelm, K., Happel, K., Eelen, G., Schoors, S., Oellerich, M.F., Lim, R., Zimmermann, B., Aspalter, I.M., Franco, C.A., Boettger, T. *et al.* (2016) FOXO1 couples metabolic activity and growth state in the vascular endothelium. *Nature*, **529**, 216–220.
55. Ghesquière, B., Wong, B.W., Kuchnio, A. and Carmeliet, P. (2014) Metabolism of stromal and immune cells in health and disease. *Nature*, **511**, 167–176.
56. Johnson, D.G., Schwarz, J.K., Cress, W.D. and Nevins, J.R. (1993) Expression of transcription factor E2F1 induces quiescent cells to enter S phase. *Nature*, **365**, 349–352.
57. Dong, P., Maddali, M.V., Srimani, J.K., Thélot, F., Nevins, J.R., Mathey-Prevot, B. and You, L. (2014) Division of labour between Myc and G1 cyclins in cell cycle commitment and pace control. *Nat. Commun.*, **5**, 4750.
58. Fang, L., Deng, Z., Shatseva, T., Yang, J., Peng, C., Du, W.W., Yee, A.J., Ang, L.C., He, C., Shan, S.W. *et al.* (2011) MicroRNA miR-93 promotes tumor growth and angiogenesis by targeting integrin-β8. *Oncogene*, **30**, 806–821.
59. Fang, L., Du, W.W., Yang, W., Rutnam, Z.J., Peng, C., Li, H., O'Malley, Y.Q., Askeland, R.W., Sugg, S., Liu, M. *et al.* (2012) MiR-93 enhances angiogenesis and metastasis by targeting LATS2. *Cell Cycle*, **11**, 4352–4365.
60. Wei, Y., Gong, J., Thimmulappa, R.K., Kosmider, B., Biswal, S. and Duh, E.J. (2013) Nrf2 acts cell-autonomously in endothelium to regulate tip cell formation and vascular branching. *Proc. Natl. Acad. Sci. U.S.A.*, **110**, E3910–E3918.
61. Dai, X., Yan, X., Zeng, J., Chen, J., Wang, Y., Chen, J., Li, Y., Barati, M.T., Wintergerst, K.A., Pan, K. *et al.* (2017) Elevating CXCR7 improves angiogenic function of EPCs via Akt/GSK-3β/Fyn-mediated Nrf2 activation in diabetic limb ischemia. *Circ. Res.*, **120**, e7–e23.
62. Feinberg, M.W. and Moore, K.J. (2016) MicroRNA regulation of atherosclerosis. *Circ. Res.*, **118**, 703–720.
63. Edgar, R., Domrachev, M. and Lash, E. (2002) Gene Expression Omnibus: NCBI gene expression and hybridization array data repository. *Nucleic Acids Res.*, **30**, 207–210.